Top Catal (2011) 54:768–777
DOI 10.1007/s11244-011-9703-0

ORIGINAL PAPER

A Highly Active and Selective Manganese Oxide Promoted Cobalt-on-Silica Fischer–Tropsch Catalyst

Johan P. den Breejen · Anne M. Frey · Jia Yang · Anders Holmen · Matti M. van Schooneveld · Frank M. F. de Groot · Odile Stephan · Johannes H. Bitter · Krijn P. de Jong

Published online: 11 August 2011

Abstract A highly active and selective manganese oxide-promoted silica-supported cobalt catalyst for the Fischer–Tropsch reaction is reported. $Co/MnO/SiO_2$ catalysts were prepared via impregnation of a cobalt nitrate and manganese nitrate precursor, followed by drying and calcination in an NO/He flow. The catalysts were studied with STEM–EELS, infrared spectroscopy measurements of adsorbed CO and Steady-State Isotopic Transient Kinetic Analysis experiments. Based on those experiments, a relation between C_{5+}-selectivity and surface-coverages of CH_x-intermediates on cobalt was found.

Electronic supplementary material The online version of this article (doi:10.1007/s11244-011-9703-0) contains supplementary material, which is available to authorized users.

J. P. den Breejen · A. M. Frey · M. M. van Schooneveld · F. M. F. de Groot · J. H. Bitter · K. P. de Jong (✉)
Department of Inorganic Chemistry and Catalysis, Debye Institute for NanoMaterials Science, Utrecht University, NL-3584 CA Utrecht, The Netherlands
e-mail: K.P.deJong@uu.nl

Present Address:
J. P. den Breejen
Shell Global Solutions International B.V., Amsterdam, The Netherlands

J. Yang · A. Holmen
Department of Chemical Engineering, Norwegian University of Science and Technology (NTNU), N-7491 Trondheim, Norway

O. Stephan
Laboratoire de Physique des Solides, Université Paris-Sud, 91405 Orsay cedex, France

Keywords Fischer–Tropsch · Cobalt on silica · Manganese promotion · NO calcination · STEM–EELS · CO adsorption · Infrared Spectroscopy · SSITKA

1 Introduction

Cobalt catalysts are extensively studied and widely applied in the Fischer–Tropsch (FT) reaction. In this reaction synthesis gas (CO/H_2) is converted into hydrocarbons, which can be used as transportation fuel. Synthesis gas can be obtained from various sources as natural gas, coal and biomass, showing the relevance of the FT reaction.

To enhance the activity of an FT catalyst per unit weight of cobalt, the latter is commonly dispersed on a support material to enhance its surface-to-volume ratio by decreasing the cobalt particle size to an optimal value of 5–6 nm. [1–4] A recent example of improving the catalytic activity using this methodology is provided in a previous contribution from our laboratory, where a cobalt-on-silica catalyst was synthesized by an impregnation and drying step, followed by calcination of cobalt nitrate precursor in a flow of NO/He [5, 6]. This method yielded a surface-weighted cobalt particle size of $\sim$5 nm with a narrow particle size distribution. As a result of that, a highly active ($4.8 \bullet 10^{-5}$ $mol_{CO}.g_{Co}.s^{-1}$ at 220 °C and 1 bar) FT catalyst was obtained, however, accompanied by a moderate C_{5+}-selectivity (32 wt%).

Aim of this study is to enhance the C_{5+}-selectivity of these small Co particles while maintaining their high activity. This was pursued by the addition of a metal oxide promoter. Various metal oxides have been used for selectivity promotion in FT catalysis, as has been reviewed by several authors [7–10]. In the current study manganese oxide was chosen. Examples of the effectiveness of this

oxide in increasing the C_{5+}-selectivity in the cobalt catalyzed FT reaction have been reported [11–23]. As an example, a study from Bezemer et al. [21] showed an increase in C_{5+}-selectivity from 31 to 45 wt% for a cobalt on carbon nanofiber catalyst upon the addition of MnO at an Mn/Co atomic ratio of 0.03. In that case MnO was added via an aqueous impregnation of manganese nitrate on a reduced and passivated Co/CNF catalyst. As this caused blocking of part of the cobalt surface, the enhancement in C_{5+}-selectivity was accompanied with a decrease in activity, which is generally observed [13–15, 17, 19–22].

In the current paper MnO-promoted Co/SiO_2 catalysts were prepared via co-impregnation using an aqueous solution of manganese nitrate and cobalt nitrate, with Mn/Co atomic ratios ranging from 0 to 0.25. After drying, the mixed nitrate samples were calcined in a flow of 1 vol% NO/He [5, 24]. Please note that this calcination method is key to obtain cobalt particles with a narrow size distribution for the unpromoted Co/SiO_2 catalyst. For comparison, other batches of dried sample were calcined in an air flow. Throughout this study Pt has been added as a reduction promoter to the catalyst.

The catalysts were characterized using X-Ray diffraction (XRD), Transmission Electron Microscopy (TEM) and Scanning Transmission Electron Microscopy with Electron Energy Loss Spectroscopy (STEM–EELS). To investigate the catalytic effect of MnO, the catalysts were tested in the FT reaction at 220 °C, $H_2/CO = 2$ v/v and atmospheric pressure. Moreover, room temperature CO adsorption monitored with infrared (IR) spectroscopy was used to indirectly probe the interaction of the supported cobalt particles and the manganese oxide. [22, 25] In addition, Steady-State Isotopic Transient Kinetic Analysis (SSITKA) was applied to study the amount and residence times of the FT intermediates CO and CH_x as a function of the amount of MnO during steady-state CO hydrogenation at 210 °C, $H_2/CO = 10$ v/v and 1.85 bar.

2 Experimental

2.1 Preparation

Silica support material (Grace-Davison Davicat 1454SI silica gel, BET surface area = 500 $m^2\ g^{-1}$, pore volume = 1.1 mL g^{-1} and 6 nm average pore size) was dried for 12 h in air at 120 °C prior to further use. MnO-promoted cobalt catalysts were prepared via a single pore-volume impregnation using an aqueous solution containing $Co(NO_3)_2{\cdot}6H_2O$, $Mn(NO_3)_2{\cdot}6H_2O$ and $Pt(NH_3)_4(NO_3)_2$, aiming for a cobalt metal loading of 17 wt%. Various catalysts were prepared with a Mn/Co atomic ratio ranging from 0 to 0.25. Platinum (0.05 wt%) was added in all cases as a reduction promoter via co-impregnation. After impregnation the catalyst was dried for 12 h at 70 °C, with a heating rate of 1 °C min^{-1}, in stagnant air. Subsequently, the dried catalyst (100 mg) was calcined for 1 h at 240 °C in a 100 mL min^{-1} flow of either 1 vol% NO in He (NC) or air (AC). The catalysts (20 mg) were reduced prior to FT catalysis with a heating rate of 5 °C.min^{-1} at temperatures ranging from 400 °C to 550 °C for 2 h, using a flow of 30 vol% H_2/He (60 mL min^{-1}). For the various characterization experiments (vide infra) similar reduction conditions were applied, followed by passivation in air at room temperature (rt).

2.2 Characterization

XRD analyses were conducted to determine the average crystallite size of the calcined catalyst precursors. The diffraction patterns were recorded by a Bruker-AXS D8 Advance X-ray diffractometer using Co-K_α radiation ($\lambda = 1.789$ Å) scanning from 10 to 90° 2θ. The Co_3O_4 crystallite sizes were determined using the Scherrer equation for the (311) peak at $2\theta = 43.1°$.

TEM measurements were performed using an FEI Technai 20F. TEM samples were prepared via an ethanol suspension of the passivated catalysts brought onto a carbon film on a copper grid.

STEM–EELS measurements were performed to investigate the spatial distribution of cobalt, manganese and silica in an AC or an NC $Co/MnO/Pt/SiO_2$ catalyst (Mn/Co = 0.08 at/at). The Co and Mn $L_{2,3}$-edges and the O K-edge were studied using a 100 keV STEM apparatus (VG HB 501) equipped with a field emission source and parallel Gatan EELS spectrometer [26, 27]. The EELS-spectra were taken with a 0.99 eV energy resolution and a 1 nm spatial resolution. The reduced (450 °C) and passivated samples were sonicated in ethanol and brought onto a carbon film on a regular copper EM grid.

X-ray Absorption Near-Edge Spectroscopy (XANES) at the Co K-edge was applied to study the degree of reduction of the catalysts. The measurements were done at DESY synchrotron (beamline C) in Hamburg, using a Si (111) double crystal monochromator detuned to 60% of the maximum intensity to avoid higher harmonics. The catalysts were reduced in situ in a transmission cell in a 30 vol% H_2 in He flow, with a ramp of 5 °C.min^{-1} at 450 °C, for 2 h. Prior to a XANES measurement the samples were cooled in the H_2/He flow to liquid nitrogen temperature. Spectra of Co_3O_4, CoO and cobalt foil were measured as references. The absorption spectra were analyzed using the XDAP code, as described elsewhere. [28, 29] The degree of reduction was calculated using linear combination analysis of the XANES spectra of the catalysts, CoO and Co foil references.

Infrared spectroscopy was used to study the adsorption of CO on the cobalt catalysts, and investigate the influence

of MnO addition. For the IR measurements, passivated catalyst (5 mg) was mixed with silica (5 mg, Davicat silicagel), pressed into a self-supporting wafer ($\sim$6 mg cm^{-2}) and mounted in an IR transmission cell. Prior to the CO adsorption measurements, the catalysts were re-reduced in an H_2 flow ($\sim$50 mL min^{-1}) at 450 °C for 2 h. Afterwards, the catalysts were cooled to room temperature. Below 100 °C, the hydrogen flow was stopped, and the cell was evacuated (10^{-6} mbar) for 15 min. Subsequently, after the admission of 350 mbar 10 vol% CO/He to the cell, several IR spectra were collected during a period of 30 min at ambient temperatures.

2.3 Catalysis

The FT reaction was performed at 220 °C at 1 bar in a plug-flow reactor with a H_2/CO ratio of 2 v/v. Typically 20 mg catalyst (90–150 μm), mixed with 200 mg SiC ($\sim$200 μm), was loaded in the reactor in order to achieve differential and isothermal plug-flow conditions. The catalysts were reduced in situ in an H_2/Ar (20/40 mL min^{-1}) flow at temperatures ranging from 400 to 550 °C for 2 h, with a ramp of 5 °C min^{-1}. Gas chromatographic analysis was performed during the FT reaction to determine the activity or Cobalt-Time-Yield (CTY, 10^{-5} $mol_{CO}.g_{Co}^{-1}$ s^{-1}) and selectivity (wt%) towards C_1- and C_{5+}-hydrocarbons. The reported activity and selectivity data are obtained after at least 20 h operation and at 2% CO conversion level, which was achieved by tuning the gas flow.

The SSITKA experiments were performed as described elsewhere [30]. Typically 100 mg catalyst (90–150 μm) was diluted with 200 mg SiC (75–150 μm) and loaded in a plug-flow microreactor. Prior to catalysis, the catalysts were reduced at 450 °C for 2 h, with a flow of 30 vol% H_2 in Ar (40 mL min^{-1}). The experiments were performed at 210 °C, 1.85 bar, with an H_2/CO ratio of 10 v/v. During steady-state reaction isotopic switches were performed, e.g., from $^{12}CO/Ar/H_2$ to $^{13}CO/Kr/H_2$. The transients of labeled reactants and products (e.g., ^{13}CO and $^{13}CH_4$) were monitored with a Mass Spectrometer (MS). The surface residence times and coverages of CO and CH_x intermediates were calculated from those transients. A gas chromatograph equipped with FID and TCD was used to determine the CO conversion.

3 Results and Discussion

3.1 XRD

In Table 1 the Co_3O_4 crystallite sizes of the calcined Co(/MnO)/Pt/SiO_2 catalyst precursors prepared via NC or AC with different Mn/Co ratios are shown.

Table 1 XRD Co_3O_4 crystallite sizes and Co particle size (nm) for AC and NC Co(/MnO)/Pt/SiO_2 catalyst precursors with various Mn/Co atomic ratios; Co loading is 17 wt% for all samples

Mn/Co ratio (at/at)	Co_3O_4 XRD crystallite size		Particle size (TEM)	
	AC	NC	AC	NC
0	9.7	4.7	12	4.6
0.06	5.8	3.3	–	3.0
0.08	4.9	3.0	–	–
0.13	5.0	3.3	–	–
0.25	4.3	3.3	5.6	3.9

Between brackets the particle size as determined with TEM analysis

As can be observed in Table 1, the air calcination treatment yields a significantly larger Co_3O_4 crystallite size for the unpromoted catalyst as compared to that obtained after calcination in a flow of NO/He. This shows the beneficial impact of NC on the Co_3O_4 crystallite size, which is in line with previous findings [5, 6, 31].

For the MnO-promoted catalysts, a smaller difference in Co_3O_4 crystallite size after either AC or NC was observed. Nevertheless, a decrease in crystallite size is observed for both NC and AC catalysts after the addition of a small amount of MnO (Mn/Co = 0.06 at/at) as compared to their unpromoted counter parts. From Table 1 it can moreover be concluded that the crystallite sizes of the Co/MnO/Pt/SiO_2 NC samples are not influenced by the amount of MnO, whereas the Co_3O_4 crystallites of the AC samples showed continuously a decreasing size with increasing MnO content. It should be noted though that the co-impregnation method is expected to yield mixed CoMn-oxides after calcination. As the Mn^{2+} ions possibly affect the stacking in the cobalt oxide crystals, domain sizes rather than crystallite sizes will be detected with XRD. This suggests that from XRD we will underestimate the crystallite sizes. In all cases no diffraction lines of MnO were detected. Please note it was assumed that the passivated catalyst contains Mn in a 2^+ oxidation state only, based on e.g., a study by Morales et al. on Co/MnO/TiO_2 catalysts. [17].

3.2 TEM

TEM analysis from reduced (450 °C) and passivated catalysts was used to investigate the cobalt particle size and distribution in more detail.

From Fig. 1a, c showing TEM images of unpromoted AC and NC Co/Pt/SiO_2 catalysts, respectively, it was concluded that a significantly higher cobalt dispersion is obtained with NO calcination as compared to air calcination. This confirms the XRD results (*cf.* Table 1). Moreover, clustering of cobalt particles is observed in the case

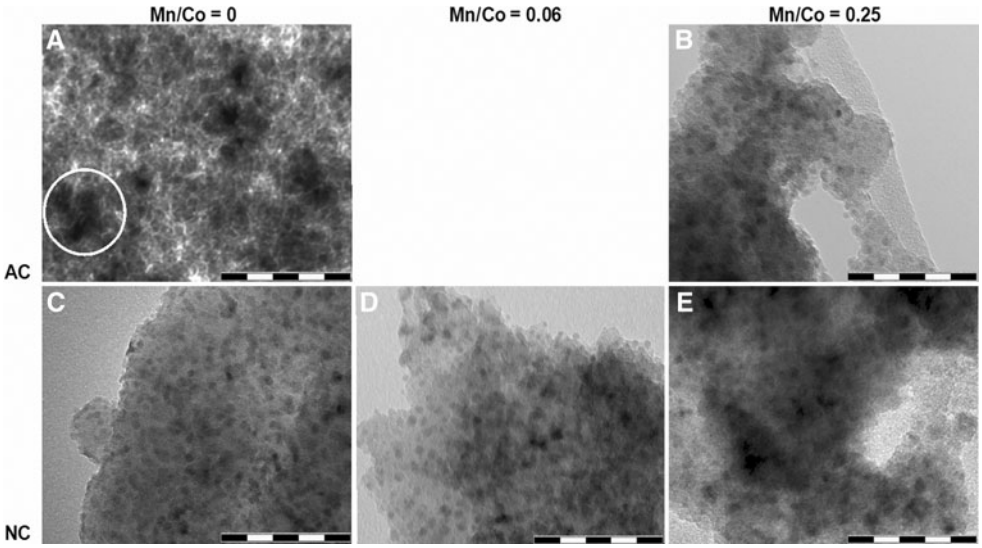

Fig. 1 TEM pictures of reduced (450 °C) and passivated AC Co(/MnO)/Pt/SiO_2 catalysts with Mn/Co ratios of 0 (**a**) and 0.25 (**b**) and NC Co(/MnO)/Pt/SiO_2 catalysts with Mn/Co ratios of 0 (**c**), 0.06 (**d**) and 0.25 (**e**). The scale bar represents 50 nm. The *white circle* in **a** indicates clustering of Co particles

of the air calcined samples (as indicated by the white circle in Fig. 1a) while the cobalt particles of the NC prepared sample (Fig. 1b) are well separated on the silica surface.

For the AC catalysts a significant improvement in cobalt dispersion is observed upon MnO addition, and a decrease in average Co particle size from 12 nm (Mn/Co = 0 at/at) to 5.6 nm (Mn/Co = 0.25 at/at, Fig. 1b) is found. However, TEM analysis on the latter sample also revealed the presence of large Co particles (>20 nm), indicating a broad particle size distribution. Nevertheless it can be concluded that the addition of manganese nitrate to impregnation solution improved the average cobalt dispersion of AC catalysts.

For the NC catalysts a small decrease in cobalt particle size is observed after MnO addition. For the MnO-promoted samples (Fig. 1c, d), small Co particles (3–4 nm, *cf.* Table 1) are obtained for both low (0.06, C) and high (0.25, D) Mn/Co atomic ratios. From the similar cobalt sizes of the promoted NC catalysts (Fig. 1c, d) it was concluded that the effect of the Mn/Co ratio on the cobalt dispersion is negligible. It should be mentioned though that due to the small difference in Co and Mn mass, a distinction between these elements in TEM could not be made, which therefore complicated an accurate cobalt particle size determination.

3.3 STEM–EELS

To investigate the spatial distribution of cobalt and manganese oxide on the silica surface after reduction and passivation, Scanning Transmission Electron Microscopy measurements combined with electron energy loss spectroscopy (STEM–EELS) were conducted. In this study the catalyst with the optimum FT performance with a Mn/Co ratio of 0.08 at/at (vide infra) prepared via NO calcination was investigated along with the corresponding air calcined sample.

In Fig. 2 composite maps of energy selected STEM images of a NO and AC sample, each measured at two spots on the sample, are shown with the spatially resolved integrated EELS intensities for oxygen, cobalt and manganese. STEM images with integrated EELS intensities for the individual elements are provided in the supplementary information.

From these images it can be concluded that a higher cobalt dispersion is obtained for the NC catalyst than for the AC catalysts, which confirms the XRD and TEM results (vide supra). Moreover, the dispersion of MnO has increased significantly upon NO calcination. Whereas relatively large particles of MnO (up to 4 nm) are formed after air calcination, often present close to the Co particles, the NO calcination seems to yield a homogeneous distribution of MnO over both the cobalt and the silica surface.

3.4 XANES

X-ray absorption spectroscopy was applied to investigate the degree of reduction. These experiments were conducted at liquid nitrogen temperature, after an in situ reduction treatment. The XANES part of these measurements on various Co(/MnO)/Pt/SiO_2 catalysts, together with Co foil and a CoO reference sample, is shown in Fig. 3.

Using linear combination analysis of CoO and Co foil reference samples, the degrees of reduction of the in situ reduced AC and NC catalysts were determined, and are listed in Table 2.

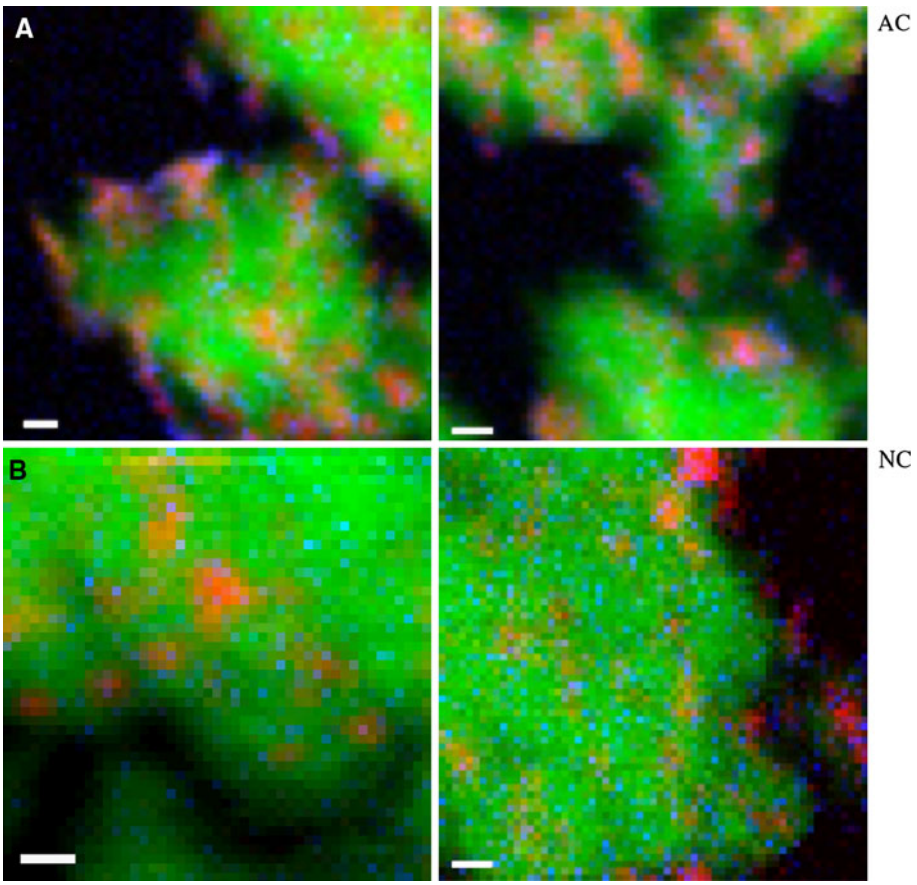

Fig. 2 STEM–EELS analysis for reduced (450 °C) and passivated AC (**a**) and NC (**b**) Co/MnO/Pt/SiO_2 catalysts (Mn/Co = 0.08 at/at), each at two different spots on the samples. The *colors* indicate the elements oxygen (*green*), cobalt (*red*) and manganese (*blue*). The *scale bar* represents 5 nm

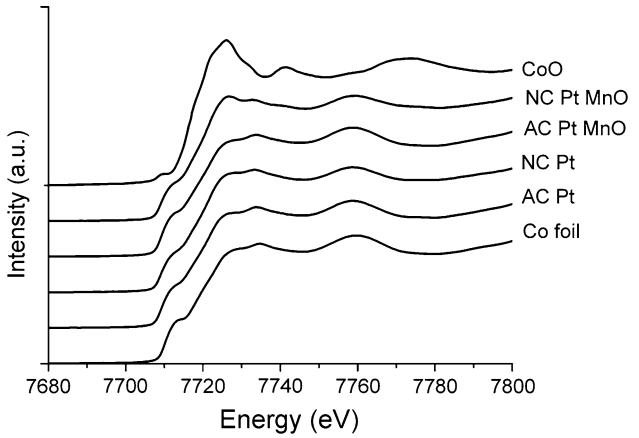

Fig. 3 XANES spectra from in situ reduced (450 °C) catalysts and the reference samples CoO and Co foil

From this table it is concluded that high degrees of reduction are obtained at 450 °C for both the AC and NC sample without MnO. Complete reduction is also achieved for the AC catalyst containing MnO (Mn/Co = 0.08 at/at). The small Co particles prepared via NO calcination, however, show a 62% degree of reduction only. Yet, this value increased to 82% after 2 h of FT synthesis (data not shown). The lower degree of reduction might be attributed to the retarding effect of MnO on the extent of reduction, as has been shown earlier e.g., for Co/MnO/TiO_2 catalysts [16].

Table 2 Degrees of reduction of Co(/MnO)/Pt/SiO_2 catalysts as obtained from XANES analysis

Catalyst	Calcination	Reduction temperature (°C)	Degree of reduction (%)
CoPt	Air	450	96 ± 5
CoPt	NO	450	96 ± 5
CoPtMnO*	Air	450	94 ± 5
CoPtMnO*	NO	450	62 ± 5

* Mn/Co = 0.08 at/at

3.5 FT catalysis

In a first series of catalysis experiments, the effect of Mn/Co ratio on the FT performance was studied. The catalysts were reduced at 550 °C to reach a degree of reduction close to 100% (vide supra).

For the CoPt/SiO_2 catalysts (no MnO present) the activity difference between NC and AC treatments is limited, and smaller than reported before [6]. Clearly, the reduction temperature applied (550 °C) is not optimal for the NC catalyst and reduction at 450 °C has been used before [6].

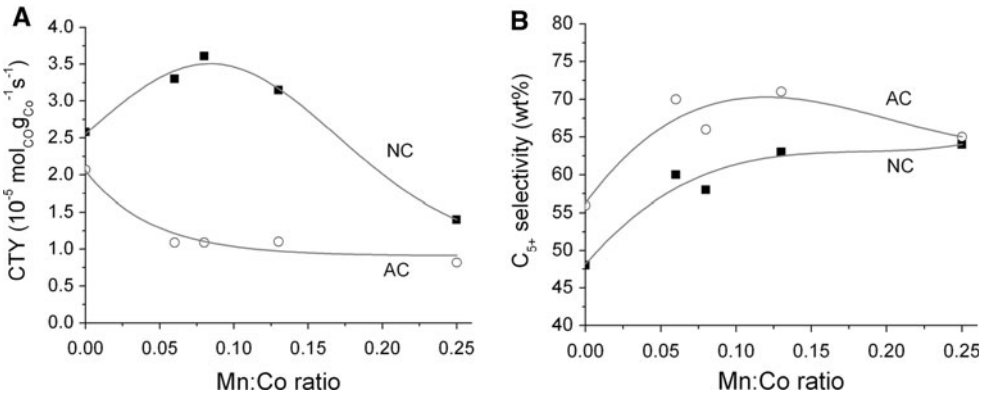

Fig. 4 Effect Mn/Co ratio on activity (**a**) and selectivity (**b**) for AC and NC Co(/MnO)/Pt/SiO_2 catalysts reduced at 550 °C

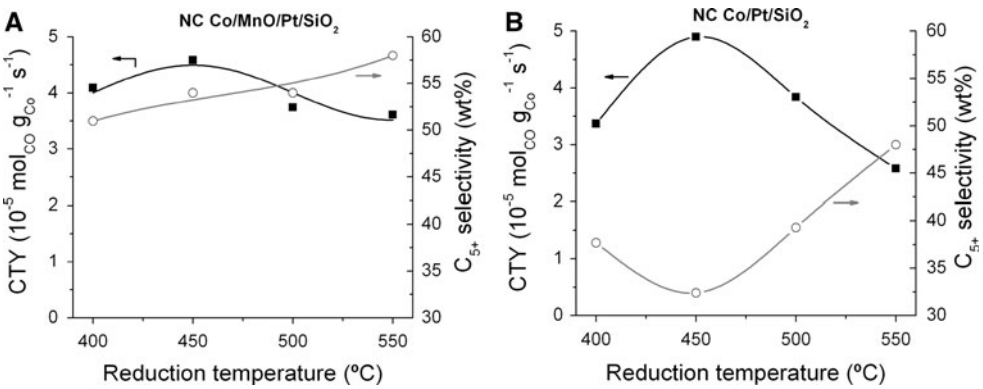

Fig. 5 Effect of the reduction temperature on activity and selectivity for (**a**) the NC $Co/MnO/Pt/SiO_2$ catalyst (Mn/Co = 0.08 at/at) and (**b**) the NC $Co/Pt/SiO_2$ catalyst

For the NC catalyst reduced at 550 °C it can be concluded that the addition of MnO up to Mn/Co = 0.08 brings about an increase of both activity (Fig. 4a) and selectivity (Fig. 4a). For larger amounts of MnO (Mn/Co > 0.13) slightly higher C_{5+}-selectivity values were found, however at a significant expense of the activity. This might be due to blockage of the cobalt surface [21] and/or a lower degree of reduction due to the reduction-retarding effect of MnO [16].

For the AC catalyst it was found that the addition of a small amount of MnO caused a decrease in activity, which value even further decreased for higher Mn/Co ratios. This might be due to blocking of the cobalt surface by MnO [21]. Nevertheless, the beneficial effect of MnO is reflected in the increase in C_{5+}-selectivity, and an increase in Mn/Co atomic ratio from 0 to 0.25 was accompanied with an increase in C_{5+}-selectivity from 56 to 70 wt%.

For the NC catalyst with the optimum amount of MnO (Mn/Co = 0.08 at/at), the effect of reduction temperature was investigated (Fig. 5a). For comparison, the effect of reduction temperature on the performance of the NC $Co/Pt/SiO_2$ catalyst without MnO was included (Fig. 5b).

From Fig. 5a it can be concluded that for NC $Co/MnO/Pt/SiO_2$ a slight increase in C_{5+}-selectivity is obtained with an increase in reduction temperature. For the activity a shallow optimum temperature of 450 °C is found. The lower activities obtained at high reduction temperatures (>450 °C) might be due to sintering.

For the unpromoted NC $Co/Pt/SiO_2$ catalyst (Fig. 5b), an initial increase in activity with increasing reduction temperature is shown. At high temperatures (>450 °C) however, a significant drop in activity is observed, which is attributed to sintering concluding from additional XRD results. It is interesting to note that the drop in activity at too high reduction temperatures (<450 °C) is larger for the $Co/Pt/SiO_2$ catalyst as compared to the $Co/MnO/Pt/SiO_2$ catalyst. This might indicate that the presence of MnO promoter inhibits sintering of the Co particles during reduction. For the $Co/Pt/SiO_2$ catalyst relatively low C_{5+}-selectivities were found, although higher values (up to 48 wt%) were obtained at higher (>450 °C) reduction temperatures possibly related to the presence of larger Co particles [2–4].

From the comparison of the NC $Co/Pt/SiO_2$ and NC $Co/MnO/Pt/SiO_2$ catalysts reduced at their optimum reduction temperature (450 °C) to obtain maximum activity it can be concluded that a significant increase in C_{5+}-selectivity (from 32 wt% to 54 wt%) is achieved by the addition of MnO. Most notably, the highest activity ($4.6 \cdot 10^{-5}$ $mol_{CO} \cdot g_{Co}^{-1}$ s^{-1}) found for the MnO promoted catalyst is close

to the value of $4.9{\cdot}10^{-5}$ $mol_{CO}.g_{Co}^{-1}$ s^{-1} obtained for the unpromoted catalyst, *cf* Fig. 5b. Moreover, this relatively high activity of the MnO promoted catalyst is obtained for Co particle sizes (~4 nm) smaller than the optimum particle size (~5 nm) [6], and hence a significantly lower activity was expected. This might indicate that the MnO promoted catalysts do not show a cobalt particle size effect identical to that of unpromoted catalyst [6], possibly caused by a different Co surface structure or particle shape. However, it might also indicate that manganese oxide acts both as selectivity and activity promoter [32], thereby boosting the performance of small Co particles.

3.6 IR Spectroscopy

IR spectroscopy of adsorbed carbon monoxide was applied to investigate the effect of MnO on the nature of the cobalt surface of NC Co(/MnO)/Pt/SiO_2 catalysts. As CO can bind to the cobalt surface in a linear, bridged and multiple-bridged form, which all have a characteristic vibrational frequency in the infrared region, detailed information about the structure and electronic properties of the surface sites can possibly be obtained [22, 33, 34]. In this study, NO-calcined Co/MnO/Pt/SiO_2 catalysts with a Mn/Co atomic ratio of 0, 0.08 and 0.13 were investigated as well as air-calcined Co/Pt/SiO_2. Prior to the IR measurements, the passivated catalyst samples were re-reduced in situ at 450 °C (see details in experimental). CO was adsorbed at ambient temperatures.

Figure 6 shows the region of the CO vibrations in the IR spectra. Small bands developed at 2,180 and 2,126 cm^{-1} are assigned to gaseous CO [22]. For the air and NO calcined Co/Pt/SiO_2, bands at 2,057 and 1,892 cm^{-1} are found, which are indicative for linear and bridged bonded CO on metallic cobalt particles, respectively [35]. From the peak areas it can be concluded that the amount of adsorbed CO on the NC catalyst is almost twice as high as on the AC catalyst, which is due to the enhanced Co dispersion. Moreover, a two times higher linear:bridge ratio of adsorbed CO is found for the NC catalyst, which might be ascribed to a higher fraction of edge and corner sites at the surfaces of the small cobalt particles in the NC sample than present at the larger particles of the AC sample. A similar effect has been observed for adsorption of CO on a defect rich Co (0001) surface, where a lower quantity of bridge-bonded CO was found as compared to the amount present on an annealed surface with a low amount of defects [36].

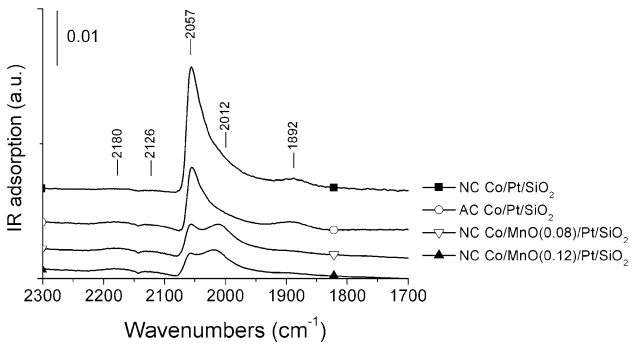

Fig. 6 Transmission IR with CO adsorption (30 °C, 30 min, 350 mbar 10 vol% CO in He)

The presence of MnO in the NC samples induced a significant change in both the CO coverage and bonding mode. This proves the close interaction of the Co particles and MnO promoter. The lower IR absorption signal indicates a lower amount of CO adsorbed on the manganese promoted catalysts, probably due to blocking of part of the Co surface by MnO [21]. Moreover, next to the peak at 2,057 cm^{-1}, a second distinct peak of linearly bonded CO is observed at around 2,012 cm^{-1} region. Whereas the first peak (2,057 cm^{-1}) is ascribed to CO adsorption on fcc cobalt [37], the latter peak has been attributed to the linear adsorption of CO on low-index surface crystallographic planes or corners and steps sites with coordinatively unsaturated sites [4, 38, 39]. This indicates that MnO-promoted catalysts exhibit a different cobalt surface structure as compared to unpromoted catalysts.

For the AC Co/Pt/SiO_2 and the MnO promoted NC catalysts higher C_{5+}-selectivities were found as compared to the C_{5+}-selectivity of the NC Co/Pt/SiO_2 catalyst. Since the AC catalyst shows a higher amount of bridged-bonded CO and the MnO promoted catalysts possibly show a different surface structure as compared to NC Co/Pt/SiO_2, it might be concluded that the C_{5+}-promoting effect of either a relatively larger Co size (AC sample) or the presence of MnO has a different origin.

3.7 SSITKA

Isotopic switches ($^{12}CO/^{13}CO$ and H_2/D_2) were applied to study the amount and residence times of various FT surface intermediates. First the carbon intermediates were investigated by a switch from $^{12}CO/Ar/H_2$ to $^{13}CO/Kr/H_2$ after reaching steady-state conversion at 210 °C, $H_2/CO = 10$ v/v and 1.85 bar. This was followed by a back-switch, after reaching an isotopic steady-state. From this back-switch, the residence times of CO and CH_x were calculated. In this case the CH_x intermediates represent the surface species which eventually produce CH_4. A detailed description of the transient analyses has been published elsewhere [30]. For AC Co/Pt/SiO_2 and NC Co(/MnO)/Pt/SiO_2 with Mn/Co atomic ratios of 0, 0.08 and 0.25 reduced at 450 °C, the amounts (N) of CO and CH_x bonded to the cobalt surface were calculated using the residence times and gas flows. (Table 3) Since part of the surface might be blocked by MnO, as the IR CO adsorption measurements suggest,

Table 3 Residence times and amounts of CO and CH_x intermediates obtained for an AC $Co/Pt/SiO_2$ and NC $Co(/MnO)/Pt/SiO_2$ catalysts with various Mn/Co ratios

	Mn/Co ratio (at/at)	τ_{CO} (s)	$\tau^{a}_{CHx,\ corr}$ (s)	N_{CO} (mmol/g_{cat})	N_{CHx} (mmol/g_{cat})	θ^{b}_{CHx}	TOF^{c}_{calc} (10^{-3} s^{-1})
AC	0	12	8.5	91	25	0.14	13
NC	0	24	4.3	174	26	0.07	15
	0.08	18	5.5	97	32	0.17	22
	0.25	9.9	7.9	76	31	0.19	17

Included are calculated CH_x and CO coverages and the TOF

[a] Corrected via: $\tau_{CHx,corr} = \tau_{CH4}–0.5\tau_{CO}$ [45]; [b]calculated as $N_{CHx}/2N_{CO}$; [c]calculated assuming $TOF_{calc} = (\theta_{CHx}/\tau_{CHx,\ corr})$ [3]

the determination of the number of Co surface sites via the cobalt dispersion is cumbersome. Hence, the CO and CH_x surface coverage on the promoted catalysts could not be calculated. Based on previous SSITKA studies using Co/CNF catalysts [3, 30] however, it was assumed that the number of cobalt surface sites equals two times the number of reversibly bonded CO. This allowed to calculate the CH_x and CO coverage via $\theta_{CHx\ or\ CO} = N_{CHx\ or\ CO}/(2N_{CO})$.

Table 3 shows that the residence time and amount of reversibly adsorbed CO on the NC $Co/Pt/SiO_2$ catalyst is twice as high as compared to the amount of CO on its air-calcined counterpart. This is in line with the IR results (vide supra) and is ascribed to the two times higher Co surface area per gram of catalyst.

For the CH_x intermediate, both a lower residence time and surface coverage was found for the NC $Co/Pt/SiO_2$ catalyst as compared to its AC counterpart. However, upon MnO addition, an increase in residence time and coverage of CH_x intermediates was observed with increasing Mn/Co ratio, which is in line with findings by Vada et al. using LaO_x promotion for a Co/Al_2O_3 catalyst [40]. At the same time, both a decrease in the residence time and amount of reversibly adsorbed CO was observed. It is interesting to note that also for ZrO_x promoted Co/Al_2O_3 catalysts an increase in CH_x-coverage and TOF is observed upon addition of the Zr promoter [41, 42]. However, in this case no change in CO coverage is observed.

From the CH_x coverage and residence time, and assuming pseudo first-order kinetics, the TOF was calculated (Table 3) [3]. The obtained values show a similar surface-specific activity for the AC and NC $Co/Pt/SiO_2$ catalyst. Interestingly, for the MnO promoted catalysts a higher calculated TOF was found, which indicates that MnO also acts as an activity promoter. This is also in line with findings for ZrO_x-promoted catalysts [41–43]. This might explain the fact that a higher selectivity of the MnO promoted NC samples was found, without showing a significant loss in activity.

In order to provide a qualitative understanding of the higher C_{5+}-selectivity of the MnO promoted catalysts and the air-calcined $Co/Pt/SiO_2$ catalysts, the CH_x coverage

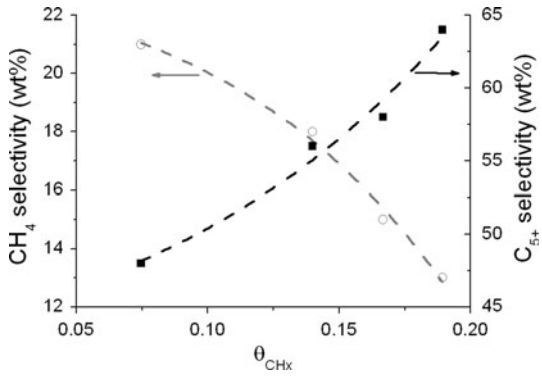

Fig. 7 CH_4- and C_{5+}-selectivities of $Co(MnO)/Pt/SiO_2$ catalysts as a function of the CH_x surface coverage

($H_2/CO = 10$, 210 °C, 1.85 bar) was plotted versus the CH_4 and C_{5+}-selectivities both determined via GC analyses ($H_2/CO = 2$, 220 °C, 1 bar) in Fig. 7.

In this figure a clear trend of increasing C_{5+}-selectivity and decreasing C_1-selectivity with increasing CH_x coverage is visible. These trends in selectivity might be rationalized by a higher C–C coupling probability with higher CH_x coverages leading to a higher C_{5+}- and lower C_1-selectivity [44].

4 Conclusions

In this paper the effect of MnO addition on the activity and C_{5+}-selectivity in FT synthesis was studied for Co/SiO_2 catalysts calcined in a flow of air or 1 vol% NO/He. For the NO calcined (NC) $Co/Mn/Pt/SiO_2$ catalysts a significantly smaller average Co size was found as compared to the air calcined samples. Moreover, as STEM–EELS data showed, this was accompanied with a significant increase in MnO dispersion. This indicates that calcination in NO/He can be applied successfully to mixed-nitrate systems. For the NC $Co/Mn/Pt/SiO_2$ catalyst with an optimum Mn/Co atomic ratio of 0.08, an increase in C_{5+}-selectivity from 32 wt% (unpromoted) to 54 wt% was found, yet without a significant loss in activity. For air-calcined (AC) $Co/Mn/Pt/SiO_2$

high C_{5+}-selectivities (up to 70 wt%) were found, although accompanied with moderate activities.

From infrared spectroscopy experiments of adsorbed carbon monoxide it was concluded that MnO blocked part of the cobalt surface. Moreover, concluding from a low-frequency band of linearly bonded CO, the presence of MnO induces the formation of cobalt surfaces with low-index crystallographic planes or steps and corners with cobalt atoms with a relatively low coordination number as compared to the unpromoted catalysts.

SSITKA results showed a decrease of both the residence time and the amount of adsorbed CO and an increase in the residence time and coverage of CH_x with increasing MnO content. Moreover, higher CH_x residence times and coverages were found for the large Co particles ($\sim$10 nm) obtained via air calcination as compared to the smaller ones ($\sim$5 nm) prepared via calcination in NO/He.

The observed increase in C_{5+}-selectivity for higher MnO loadings was attributed to the increase in the CH_x coverage, bringing about a higher C–C coupling probability.

5 Supporting information

High Angle Annular Dark Field (HAADF) images for an AC and NC Co/Pt/MnO/SiO_2 catalyst (Mn/Co = 0.08 at/at) together with the spatially resolved EELS intensities for oxygen, cobalt and manganese.

Acknowledgments The authors thank Dr. A. Gloter, Dr. I. Swart and Dr. A. Juhin for their help with and also the Université de Nord (Paris) for the possibility of performing STEM–EELS measurements. C. van der Spek and Prof. Dr. Ir. J.W. Geus are thanked for the TEM analyses. Scientists from beamline C, HASYLAB synchrotron (I20070099 EC) are thanked for their assistance in the XAS experiments. Shell Global Solutions is acknowledged for financial support.

References

1. Barbier A, Tuel A, Arcon I, Kodre A, Martin GA (2001) J Catal 200:106–116
2. Bezemer GL, Bitter JH, Kuipers HPCE, Oosterbeek H, Holewijn JE, Xu X, Kapteijn F, Van Dillen AJ, De Jong KP (2006) J Am Chem Soc 128:3956–3964
3. den Breejen JP, Radstake PB, Bezemer GL, Bitter JH, Frøseth V, Holmen A, de Jong KP (2009) J Am Chem Soc 131:7197–7203
4. Prieto G, Martínez A, Concepción P, Moreno-Tost R (2009) J Catal 266:129–144
5. Sietsma JRA, Meeldijk JD, den Breejen JP, Versluijs-Helder M, van Dillen AJ, de Jongh PE, de Jong KP (2007) Angew Chem Int Ed 46:4547–4549
6. den Breejen JP, Sietsma JRA, Friedrich H, Bitter JH, de Jong KP (2010) J Catal 270:146–152
7. Morales F, Weckhuysen BM (2006) Catalysis (R Soc Chem) 19:1
8. Khodakov AY, Chu W, Fongarland P (2007) Chem Rev 107:1692–1744
9. Anderson RB (1984) The Fischer-Tropsch synthesis. Academic Press, Orlando
10. Oukaci R, Singleton AH, Goodwin JG (1999) Appl Catal A 186:129–144
11. Van Der Riet M, Hutchings GJ, Copperthwaite RG (1986) J Chem Soc, Chem Commun 10:798–799
12. Kanai H, Tan BJ, Klabunde KJ (1986) Langmuir 2:760–765
13. Colley S, Copperthwaite RG, Hutchings GJ, Van Der Riet M (1988) Ind Eng Chem Res 27:1339–1344
14. Zhang JL, Ren J, Chen JG, Sun YH (2002) Acta Phys-Chim Sin 18:260–263
15. Keyser MJ, Everson RC, Espinoza RL (1998) Appl Catal A: Gen 171:99–107
16. Morales F, De Groot FMF, Glatzel P, Kleimenov E, Bluhm H, Honecker M, Knop-Gericke A, Weckhuysen BM (1620) J Phys Chem B 108(2004):1–16207
17. Morales F, De Groot FMF, Gijzeman OLJ, Mens A, Stephan O, Weckhuysen BM (2005) J Catal 230:301–308
18. Morales F, Grandjean D, De Groot FMF, Stephan O, Weckhuysen BM (2005) Phys Chem Chem Phys 7:568–572
19. Duvenhage DJ, Coville NJ (2005) Catal Lett 104:129–133
20. Bezemer GL, Falke U, Van Dillen AJ, De Jong KP (2005) Chem Commun 6:731–733
21. Bezemer GL, Radstake PB, Falke U, Oosterbeek H, Kuipers HPCE, Van Dillen AJ, De Jong KP (2006) J Catal 237:152–161
22. Morales F, de Smit E, de Groot FMF, Visser T, Weckhuysen BM (2007) J Catal 246:91–99
23. Feltes TE, Espinosa-Alonso L, Smit Ed, D'Souza L, Meyer RJ, Weckhuysen BM, Regalbuto JR (2010) J Catal 270:95–102
24. Sietsma JRA, van Dillen AJ, de Jongh PE, de Jong KP.(2006) GB0617529.3
25. Jiang M, Koizumi N, Ozaki T, Yamada M (2001) Appl Catal A: Gen 209:59–70
26. Stéphan O, Gloter A, Imhoff D, Kociak M, Mory C, Suenaga K, Tencé M, Colliex C (2000) Surf Rev Lett 7:475–494
27. van Schooneveld MM, Gloter A, Stephan O, Zagonel LF, Koole R, Meijerink A, Mulder WJM, de Groot FMF (2010) Nat Nanotechnol 5:538
28. Vaarkamp M, Linders JC, Koningsberger DC (1995) Physica B 209:159–160
29. Koningsberger DC, Mojet BL, van Dorssen GE, Ramaker DE (2000) Top Catal 10:143–155
30. Frøseth V, Storsæter S, Borg O, Blekkan EA, Rønning M, Holmen A (2005) Appl Catal A: Gen 289:10–15
31. Jacobs G, Ma W, Ji Y, Khalid S, Davis BH (2008) Prepr Pap-Am Chem Soc, Div Petr Chem 53:80
32. Klabunde KJ, Imizu Y (1984) J Am Chem Soc 106:2721–2722
33. Mojet BL, Miller JT, Koningsberger DC, Phys J (1999) Chem B 103:2724–2734
34. Oosterbeek H (2007) Phys Chem Chem Phys 9:3570
35. Hoffmann FM (1983) Surf Sci Rep 3:107
36. Beitel GA, Laskov A, Oosterbeek H, Kuipers EW (1996) J Phys Chem 100:12494–12502
37. Song D, Li J, Cai Q (2007) J Phys Chem C 111:18970–18979
38. Blyholder G (1964) J Phys Chem 68:2772–2777
39. Rygh LES, Nielsen CJ (2000) J Catal 194:401–409
40. Vada S, Chen B, Goodwin JG (1995) J Catal 153:224–231

41. Jongsomjit B, Panpranot J, Goodwin JG Jr (2003) J Catal 215:66–77
42. Rohr F, Holmen A, Barbo KK, Warloe P, Blekkan EA (1998) Stud Surf Sci Cat 119:107–112
43. Ali S, Chen B, Goodwin JG Jr (1995) J Catal 157:35–41
44. Bertole CJ, Kiss G, Mims CA (2004) J Catal 223:309–318
45. Biloen P, Helle JN, van den Berg FGA, Sachtler WMH (1983) J Catal 81:450–463